LETTERS
https://doi.org/10.1038/s41566-019-0395-5
nature photonics

An optical tweezer phonon laser

Robert M. Pettit[1,2*], Wenchao Ge[3*], P. Kumar[3], Danika R. Luntz-Martin[2,4], Justin T. Schultz[1,2], Levi P. Neukirch[5], M. Bhattacharya[2,3*] and A. Nick Vamivakas[1,2,4,6*]

Phonon lasers are mechanical analogues of the ubiquitous optical laser and have been realized in a variety of contexts[1–12]. However, no such demonstration exists for mesoscopic levitated optomechanical systems, which are emerging as important platforms for conducting fundamental tests of quantum mechanics[13–15] and gravity[16], as well as for developing sensing modalities that couple mechanical motion to electron spin[17–20] and charge[21]. Inspired by the pioneering work of Arthur Ashkin on optical tweezers[22,23], we introduce a mesoscopic, frequency-tunable phonon laser based on the centre-of-mass oscillation of a silica nanosphere levitated in an optical tweezer under vacuum. Unlike previous levitated realizations, our scheme is general enough to be used on single electrons, liquid droplets or even small biological organisms[24]. Our device thus provides a pathway for a coherent source of phonons on the mesoscale that can be applied to both fundamental problems in quantum mechanics as well as tasks of precision metrology[25–27].

The study of coherence, as a fundamental phenomenon as well as an enabler of technology, is a major research area in contemporary physics[28]. In the context of mesoscopic levitated optomechanical systems, efforts to prepare (ground-state) quantum coherence are under way[29,30] and parametrically driven classical systems have been studied[31–33]. However, no demonstration of laser-like coherence yet exists. Successful implementations with trapped ions have utilized Doppler forces resulting from optical beams red- and blue-detuned from an atomic resonance[4]; however, this method fails if the levitated object has no discrete internal energy structure.

In this Letter we demonstrate a levitated optomechanical analogue to an optical laser. The dynamics result from the controlled interplay of loss, gain and nonlinearity. A phase transition from Brownian motion to sustained coherent oscillation is observed with a clear threshold between the two regimes. Phonon laser systems have previously been explored in atomic systems (mass $\sim 1\times10^{-25}$ kg) and microscale (mass $\sim 1\times10^{-9}$ kg) oscillators[1–12]. Here we provide the first step towards the generation of coherent as well as nonclassical states of motion in levitated mesoscopic systems (mass $\sim 1\times10^{-18}$ kg) that also exhibit in situ frequency tunabiliy.

The experimental apparatus is based on a free-space optical dipole trap as illustrated in Fig. 1 (see Supplementary Section 1 for more details). Light scattering provides a position measurement that is processed to derive feedback signals that control the centre-of-mass dynamics. One signal provides nonlinear parametric cooling of centre-of-mass phonons, while the other induces linear amplification of centre-of-mass phonons. The feedback-induced nonlinearity is tunable, and allows for control over the steady-state phonon population, in principle into the quantum regime[29]. Furthermore, the specific form of the feedback nonlinearity is chosen to realize a near-perfect analogy to the canonical optical laser[34] (for which scientists have accumulated over 50 years of experience). Finally, we note that our feedback technique does not rely on any internal resonances of the nanoparticle, unlike ionic experiments[4]. The inset in Fig. 1 shows density maps of the particle's position in the plane transverse to beam propagation below (left) and above (right) the oscillation threshold, respectively. The left inset shows Brownian motion with a centre-of-mass temperature of 250 mK for each axis, while the right inset shows a double-lobed pattern indicative of the induced coherent oscillation along the x axis.

The system is modelled by a master equation that includes the unitary dynamics of the oscillator, diffusive and dissipative interactions with the environment and the effects of feedback (including backaction). The master equation is discussed in Supplementary Section 2 and is used to derive a dynamical equation for the mean phonon population in a single oscillatory mode

$$\langle \dot{N} \rangle = C\langle N\rangle - B\langle N\rangle^2 + A \tag{1}$$

in which $N \equiv b^\dagger b$ is the phonon occupation number of the mode where b ($b^\dagger$) is the phonon annihilation (creation) operator. $\langle N\rangle$ is related to measurable quantities through the relationship $\langle N\rangle = M\Omega_0\langle x^2\rangle/\hbar$, where M is the mass of the levitated particle, Ω_0 is the oscillation frequency of the mode, x is the displacement of the particle's centre of mass with respect to the centre of the trap, and $\hbar$ is the reduced Planck's constant. The coefficients are $A=\gamma_a+D_t-6\gamma_c$, $B=24\gamma_c$ and $C=2(\gamma_a-\gamma_g-12\gamma_c)$ where parameters γ_a, γ_c and γ_g represent the rates associated with linear feedback amplification, nonlinear feedback cooling and gas damping, respectively, while D_t incorporates diffusion due to optical and gas scattering. All parameters are experimentally controllable. Importantly, for the oscillation amplitudes considered here, there is no coupling between the particle's three modes of oscillation.

Equation (1) makes a direct connection to single-mode optical laser theory[34]. The first term on the right-hand side ($\propto\langle N\rangle$) produces amplification of centre-of-mass phonons above threshold: $\gamma_a > \gamma_g + 12\gamma_c$. This amplification is proportional to the mean phonon population, analogous to stimulated photon emission. The second term on the right-hand side ($\propto\langle N\rangle^2$) provides nonlinearity leading to saturation of the amplification and stability of the oscillator. The third term is responsible for phonon number fluctuations and is not present in classical optical models[34]. It allows the mean phonon population to build up even if $\langle N\rangle = 0$.

We demonstrate threshold behaviour in Fig. 2a by increasing the modulation depth of the amplification feedback signal $M_a = \delta P_a/P_0$, where P_0 is the power of the trapping beam and δP_a

[1]Institute of Optics, University of Rochester, Rochester, NY, USA. [2]Center for Coherence and Quantum Optics, University of Rochester, Rochester, NY, USA. [3]School of Physics and Astronomy, Rochester Institute of Technology, Rochester, NY, USA. [4]Department of Physics and Astronomy, University of Rochester, Rochester, NY, USA. [5]Los Alamos National Laboratory, Los Alamos, NM, USA. [6]Materials Science Program, University of Rochester, Rochester, NY, USA. *e-mail: rpettit@ur.rochester.edu; wenchaoge.tamu@gmail.com; mxbsps@rit.edu; nick.vamivakas@rochester.edu

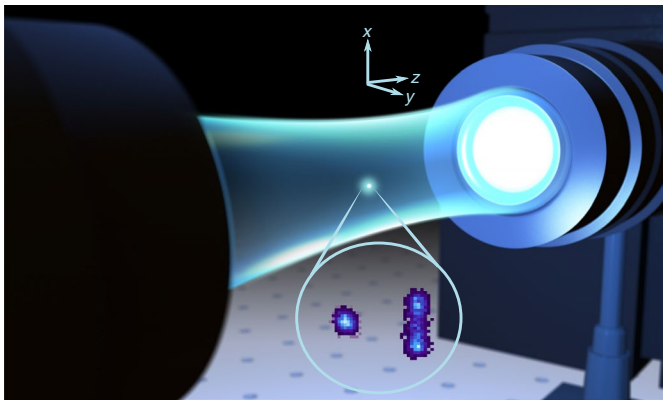

Fig. 1 | Optical tweezer illustration and system model. Artistic rendering of a silica nanosphere levitated in vacuum by an optical tweezer. Inset: motion of the levitated sphere's centre of mass observed in the plane transverse to beam propagation, showing Brownian motion below threshold (left) and coherent oscillation along the *x* axis above threshold (right).

is the power modulation induced by the feedback amplification, for various set values of γ_c at a constant pressure of 6×10^{-5} mbar (gas scattering dominates over radiation pressure shot noise). We infer feedback amplification rates from the modulation depth by $\gamma_a = M_a\Omega_0$ and feedback cooling rates from the steady-state phonon population without amplification[29]. Increasing γ_c has the effect of reducing the phonon population of the oscillatory mode. For the data presented in Fig. 2a, γ_c was tuned for the trap's *x* axis, thereby tuning the initial steady-state phonon population, before the feedback amplification was turned on. The oscillation frequency along the trap's *x* axis is $\Omega_0 = 2\pi\times128.5$ kHz. All three data sets are compared with a steady-state solution to equation (1) obtained by taking $\langle\dot{N}\rangle = 0$, which yields

$$\langle N\rangle_{ss} = \frac{1}{2B}\left(C+\sqrt{C^2+4AB}\right) \tag{2}$$

Each value of γ_c therefore provides a unique threshold condition for the phonon laser as M_a is increased, and, since the trap d.c. optical power controls the oscillation frequency, it is possible to frequency-tune the optical tweezer phonon laser. Figure 2b illustrates this capability for three different optical powers.

In Fig. 2c we examine the steady-state statistics of the system in more detail and show the second-order phonon autocorrelation function at zero time delay, $g^{(2)}(0) = (\langle N^2\rangle - \langle N\rangle)/\langle N\rangle^2$, where $\langle N^2\rangle$ is the second moment of the distribution. Note that $g^{(2)}(0) = 2$ for a thermal state and $g^{(2)}(0) = 1$ for a coherent state[35]. Experimental distributions were recorded by monitoring oscillator dynamics in a time window of 20 ms for each value of M_a. The length of the error bars represents ±1 s.d. of 100 such measurements. The solid lines represent the theoretical expectation for our system. Below threshold, $g^{(2)}(0) = 2$, confirming the expected thermal statistics. Once the feedback amplification rate greatly exceeds the threshold value, $g^{(2)}(0)$ approaches 1, which is expected for a laser operating far above threshold. For the case of $\gamma_c/(2\pi) = 4.4\times10^{-4}$ Hz, the recorded data deviate slightly from the theoretical expectation for higher values of M_a, probably due to phase error in the electronic feedback system.

Figure 2d presents two of the measured phonon probability distributions used in Fig. 2c. Markers (i) and (ii) indicate distributions recorded for M_a below and far above threshold, respectively. Below threshold the distribution is well described by a thermal Boltzmann distribution, but as the amplification rate is increased through threshold the statistics change. Far above threshold the distribution shifts and is centred about the mean. However, the observed statistics far above threshold are not Poissonian. The distributions we observe are characterized by a variance that is greater than the mean and well described by a Gaussian distribution truncated at $n = 0$. Such a distribution is predicted by our theoretical modelling (Supplementary Section 2.3) to be

$$P(n) = \frac{1}{\sqrt{\pi n_{max}}}\exp\left(-\frac{(n-n_0)^2}{n_{max}}\right) \tag{3}$$

where $n_0 = \langle N\rangle$, $n_{max} = 2n_0Q_M$ and Q_M is the Mandel *Q* parameter where $Q_M = n_0(g^{(2)}(0)-1)$. Using the measured values of $g^{(2)}(0)$, the phonon probability distribution far above threshold in Fig. 2d is well matched by equation (3). We note that the variance of the distribution is smaller than that of a thermal state with the same mean phonon number, indicating subthermal number squeezing. Higher degrees of subthermal number squeezing, leading to Poissonian phonon statistics, are predicted by our model for chamber pressures on the order of 1×10^{-8} mbar and feedback amplification rates similar to those demonstrated in this Letter.

For the same cases (i) and (ii), we examine the steady-state phase-space distributions of the oscillator (Fig. 2e) by measuring the in-phase and quadrature components of the oscillator's motion with a lock-in amplifier. The top panels show data, while the bottom panels show theoretical expectations based on the oscillator's *P*-function representation (Supplementary Section 3). The axes are defined by the coordinates *Q* and *P*, where $Q = q/q_0$ and $P = p/p_0$ are the in-phase and quadrature components of the motion scaled by the zero point position and momentum spread of the oscillator. Below threshold the *P*-function is that of a thermal state, while far above threshold the *P*-function, close to that of a coherent state, can be expressed using equation (3) by substituting $n \to (Q^2+P^2)/2$.

The transient dynamics of the system as the gain is switched on along the trap's *x* axis are explored in Fig. 3. After a period of amplification, the gain was switched off and the oscillator was allowed to cool under the influence of the feedback cooling loop to re-initialize the state of the particle. Repetition of this cycle through 500 iterations allowed statistical distributions of the oscillator's phonon population to be constructed as the system evolved, and from these distributions the mean could be calculated. In Fig. 3a, the mean phonon occupation of the mode is monitored over a window of 200 ms, including the point at which the gain is turned on at a time $t = 0$, for two different values of M_a above threshold. The obtained data can be tested against the time-dependent solution to equation (1)

$$\langle N(t)\rangle = \frac{C}{2B}+\frac{1}{B\tau}\tanh\left(\frac{t}{\tau}+\theta\right) \tag{4}$$

where $\theta = \tanh^{-1}(\tau(BN_0 - C/2))$, N_0 is the initial phonon population, and the characteristic timescale is $\tau = 2(C^2+4AB)^{-1/2}$. Good agreement is found between both experiment and theory in Fig. 3a. In each case, the initial phonon population was $N_0 = 5.75\pm0.23\times10^4$, and on application of the linear gain, the population experienced a period of exponential growth followed by saturation due to the nonlinear feedback cooling, finally reaching the steady-state value. The evolution of the phonon probability distribution can be monitored from the obtained data and compared against theoretical expectations (Fig. 3b). Distributions for various delays after the linear gain was switched on are shown for the case where $M_a = 5.6\times10^{-3}$. The distribution is shown to evolve from a thermal Boltzmann distribution in case (i) to a distribution well described by equation (3) in case (iv) when the phonon laser reaches the steady state. In cases (ii) and (iii), the theoretical expectations are computed from the Fokker–Planck equation (Supplementary Section 3).

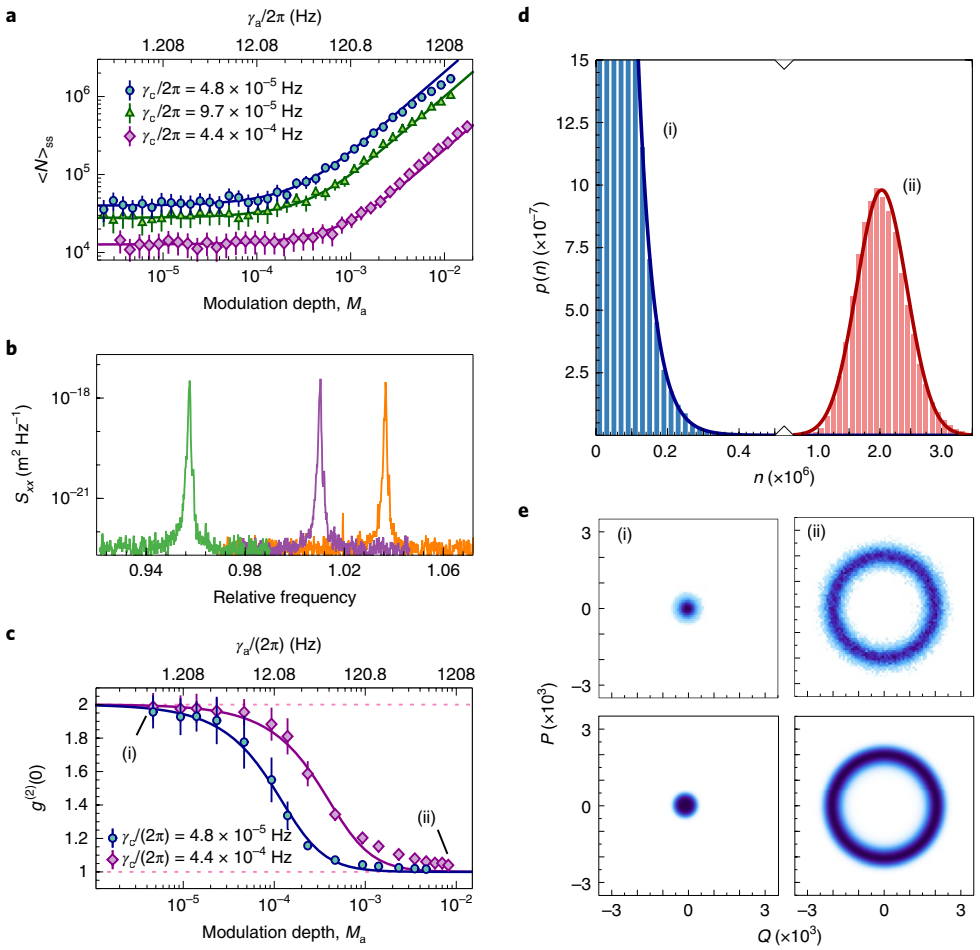

Fig. 2 | Steady-state properties. a, The mean phonon population of the oscillation as a function of the amplifying modulation depth, M_a, for different values of the feedback cooling rate, γ_c. Solid lines are theoretical expectations based on equation (2). Error bars represent one standard deviation (s.d.) of each measurement, consisting of 282,700 samples. **b**, In situ tuning of the single-mode phonon laser frequency, normalized by the mean of the two outlying spectra. Optical powers considered are 72 mW, 80 mW and 85 mW. **c**, Second-order phonon autocorrelation function at zero delay, $g^{(2)}(0)$, as M_a is increased across the threshold for two different values of the feedback cooling rate, γ_c. Error bars represent s.d. from 100 measurements. The dotted lines at $g^{(2)}(0) = 2$ and 1 indicate the expected values for a thermal state and a coherent state, respectively, while the solid lines are theoretical expectations. Markers (i) and (ii) indicate values of M_a where the oscillator is below and above threshold, respectively. **d**, Phonon probability distributions for the selected values of M_a. Solid lines are theoretical expectations for (i) a Boltzmann distribution and (ii) a distribution based on equation (3). The horizontal axis is split to better show both distributions. **e**, Comparison of experimentally measured quadratures of the oscillator's motion (top) with theoretically expected phase-space distribution based on the P-function (bottom) for the selected values of M_a. A phase transition between (i) Brownian motion and (ii) coherent oscillation is evident.

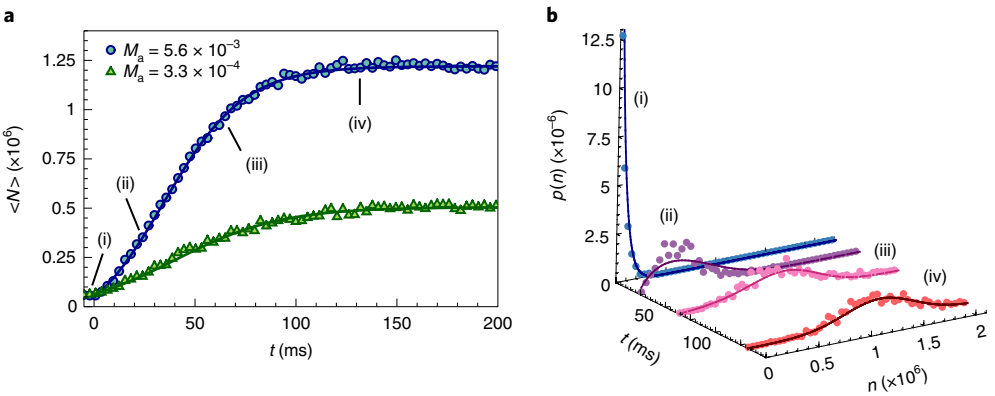

Fig. 3 | Transient behaviour after the linear gain is switched on. a, Mean phonon population monitored in time for two different values of M_a, calculated from 500 experimental iterations of the switching experiment in which the linear gain is switched on at time $t = 0$. Solid curves are theoretical expectations based on equation (4), and the markers indicate the system's evolution at (i) 0 ms, (ii) 23.7 ms, (iii) 62.2 ms and (iv) 130.5 ms from the time the gain was switched on. **b**, Evolution of the oscillator's phonon probability distribution shown for the selected times. Solid curves are theoretical expectations for (i) a Boltzmann distribution, (ii,iii) distributions based on solutions of the Fokker–Planck equation and (iv) a distribution based on equation (3) in the steady state.

In this Letter we have introduced a levitated nanoparticle phonon laser using an optical tweezer. We have presented experimental evidence for threshold behaviour and saturation, frequency tunability, as well as subthermal number squeezing by measuring phonon autocorrelations of $g^2(0) \sim 1$. Both transient and steady-state data are in excellent agreement with a theoretical model that includes spontaneous as well as stimulated emission of phonons. We expect the development of this phonon laser to have applications for levitated mechanical systems analogous to those that the opical laser has for optics. These could therefore include metrology[36], non-classical state engineering[37] and information processing[38]. Our technique is general, requiring only the ability to perform position measurement and feedback on a mechanical oscillator with a high quality factor, and therefore can be readily extended to other levitated or mechanically clamped optomechanical systems.

Online content

Any methods, additional references, Nature Research reporting summaries, source data, statements of data availability and associated accession codes are available at https://doi.org/10.1038/s41566-019-0395-5.

Received: 15 October 2018; Accepted: 20 February 2019;
Published online: 1 April 2019

References

1. Wallentowitz, S., Vogel, W., Siemers, I. & Toschek, P. E. Vibrational amplification by stimulated emission of radiation. *Phys. Rev. A* **54**, 943–946 (1996).
2. Liu, H. C. et al. Coupled electron–phonon modes in optically pumped resonant intersubband lasers. *Phys. Rev. Lett.* **90**, 077402 (2003).
3. Bargatin, I. & Roukes, M. L. Nanomechanical analog of a laser: amplification of mechanical oscillations by stimulated Zeeman transitions. *Phys. Rev. Lett.* **91**, 138302 (2003).
4. Vahala, K. et al. A phonon laser. *Nat. Phys.* **5**, 682–686 (2009).
5. Beardsley, R. P., Akimov, A. V., Henini, M. & Kent, A. J. Coherent terahertz sound amplification and spectral line narrowing in a Stark ladder superlattice. *Phys. Rev. Lett.* **104**, 085501 (2010).
6. Grudinin, I. S., Lee, H., Painter, O. & Vahala, K. J. Phonon laser action in a tunable two–level system. *Phys. Rev. Lett.* **104**, 083901 (2010).
7. Kabuss, J., Carmele, A., Brandes, T. & Knorr, A. Optically driven quantum dots as source of coherent cavity phonons: a proposal for a phonon laser scheme. *Phys. Rev. Lett.* **109**, 054301 (2012).
8. Jing, H. et al. PT-symmetric phonon laser. *Phys. Rev. Lett.* **113**, 053604 (2014).
9. Lü, H., Özdemir, S. K., Kuang, L.-M., Nori, F. & Jing, H. Exceptional points in random-defect phonon lasers. *Phys. Rev. Appl.* **8**, 044020 (2017).
10. Wang, G. et al. Demonstration of an ultra-low-threshold phonon laser with coupled microtoroid resonators in vacuum. *Photon. Res.* **5**, 73–76 (2017).
11. Zhang, J. et al. A phonon laser operating at an exceptional point. *Nat. Photon.* **12**, 479–484 (2018).
12. Ip, M. et al. Phonon lasing from optical frequency comb illumination of trapped ions. *Phys. Rev. Lett.* **121**, 043201 (2018).
13. Scala, M., Kim, M. S., Morley, G. W., Barker, P. F. & Bose, S. Matter-wave interferometry of a levitated thermal nano-oscillator induced and probed by a spin. *Phys. Rev. Lett.* **111**, 180403 (2013).
14. Yin, Z.-q., Li, T., Zhang, X. & Duan, L. M. Large quantum superpositions of a levitated nanodiamond through spin-optomechanical coupling. *Phys. Rev. A* **88**, 033614 (2013).
15. Bateman, J., Nimmrichter, S., Hornberger, K. & Ulbricht, H. Near-field interferometry of a free-falling nanoparticle from a point-like source. *Nat. Commun.* **5**, 4788 (2014).
16. Bose, S. et al. Spin entanglement witness for quantum gravity. *Phys. Rev. Lett.* **119**, 240401 (2017).
17. Neukirch, L. P., Gieseler, J., Quidant, R., Novotny, L. & Vamivakas, A. N. Observation of nitrogen vacancy photoluminescence from an optically levitated nanodiamond. *Opt. Lett.* **38**, 2976–2979 (2013).
18. Neukirch, L. P., von Haartman, E., Rosenholm, J. M. & Vamivakas, A. N. Multi-dimensional single-spin nano-optomechanics with a levitated nanodiamond. *Nat. Photon.* **9**, 653–657 (2015).
19. Hoang, T. M., Ahn, J., Bang, J. & Li, T. Electron spin control of optically levitated nanodiamonds in vacuum. *Nat. Commun.* **7**, 12250 (2016).
20. Pettit, R. M., Neukirch, L. P., Zhang, Y. & Vamivakas, A. N. Coherent control of a single nitrogen-vacancy center spin in optically levitated nanodiamond. *J. Opt. Soc. Am. B* **34**, C31–C35 (2017).
21. Millen, J., Fonseca, P. Z. G., Mavrogordatos, T., Monteiro, T. S. & Barker, P. F. Cavity cooling a single charged levitated nanosphere. *Phys. Rev. Lett.* **114**, 123602 (2015).
22. Ashkin, A. & Dziedzic, J. M. Optical levitation in high vacuum. *Appl. Phys. Lett.* **28**, 333–335 (1976).
23. Ashkin, A., Dziedzic, J. M., Bjorkholm, J. E. & Chu, S. Observation of a single-beam gradient force optical trap for dielectric particles. *Opt. Lett.* **11**, 288–290 (1986).
24. Romero-Isart, O. et al. Large quantum superpositions and interference of massive nanometer-sized objects. *Phys. Rev. Lett.* **107**, 020405 (2011).
25. Geraci, A. A., Papp, S. B. & Kitching, J. Short-range force detection using optically cooled levitated microspheres. *Phys. Rev. Lett.* **105**, 101101 (2010).
26. Ranjit, G., Cunningham, M., Casey, K. & Geraci, A. A. Zeptonewton force sensing with nanospheres in an optical lattice. *Phys. Rev. A* **93**, 053801 (2016).
27. Hempston, D. et al. Force sensing with an optically levitated charged nanoparticle. *Appl. Phys. Lett.* **111**, 133111 (2017).
28. Streltsov, A., Adesso, G. & Plenio, M. B. Colloquium: quantum coherence as a resource. *Rev. Mod. Phys.* **89**, 041003 (2017).
29. Rodenburg, B., Neukirch, L. P., Vamivakas, A. N. & Bhattacharya, M. Quantum model of cooling and force sensing with an optically trapped nanoparticle. *Optica* **3**, 318–323 (2016).
30. Jain, V. et al. Direct measurement of photon recoil from a levitated nanoparticle. *Phys. Rev. Lett.* **116**, 243601 (2016).
31. Gieseler, J., Quidant, R., Dellago, C. & Novotny, L. Dynamic relaxation of a levitated nanoparticle from a non-equilibrium steady state. *Nat. Nanotechnol.* **9**, 358–364 (2014).
32. Gieseler, J., Spasenović, M., Novotny, L. & Quidant, R. Nonlinear mode coupling and synchronization of a vacuum-trapped nanoparticle. *Phys. Rev. Lett.* **112**, 103603 (2014).
33. Gieseler, J., Novotny, L., Moritz, C. & Dellago, C. Non-equilibrium steady state of a driven levitated particle with feedback cooling. *New J. Phys.* **17**, 045011 (2015).
34. Scully, M. O. & Zubairy, M. S. in *Quantum Optics* 327–361 (Cambridge Univ. Press, 1997).
35. Gerry, C. C. & Knight, P. L. in *Introductory Quantum Optics* 115–134 (Cambridge Univ. Press, 2005).
36. Udem, T., Holzwarth, R. & Hänsch, T. W. Optical frequency metrology. *Nature* **416**, 233–237 (2002).
37. Dell'Anno, F., De Siena, S. & Illuminati, F. Multiphoton quantum optics and quantum state engineering. *Phys. Rep.* **428**, 53–168 (2006).
38. Ourjoumtsev, A., Tualle-Brouri, R., Laurat, J. & Grangier, P. Generating optical Schrödinger kittens for quantum information processing. *Science* **312**, 83–86 (2006).

Acknowledgements

R.M.P., D.R.L-M., J.T.S. and A.N.V. acknowledge generous support from the Institute of Optics and the Department of Physics and Astronomy at the University of Rochester and Office of Naval Research awards N00014-17-1-2285 and N00014-18-1-2370. W.G., P.K. and M.B. acknowledge support from Office of Naval Research awards N00014-14-1-0803 and N00014-17-1-2291 and useful discussions with J. Lawall and A.K. Jha.

Author contributions

M.B. and A.N.V. conceived the research. W.G. and P.K. performed the theoretical calculations, guided by M.B. R.M.P. performed the measurements. All authors discussed the data and wrote the manuscript.

Competing interests

The authors declare no competing interests.

Additional information

Supplementary information is available for this paper at https://doi.org/10.1038/s41566-019-0395-5.

Reprints and permissions information is available at www.nature.com/reprints.

Correspondence and requests for materials should be addressed to R.M.P., W.G., M.B. or A.N.V.

Publisher's note: Springer Nature remains neutral with regard to jurisdictional claims in published maps and institutional affiliations.

Methods

Nanosphere preparation and trapping. Silica nanospheres with a nominal diameter of 150 nm were purchased from MSP Corporation (NanoSilica NS-0150A) in aqueous suspension. Before trapping, approximately 40 µl of the suspension was dispersed into 1 ml of absolute ethanol and sonicated for 2 min. The dispersed solution was then further diluted with an additional 1 ml of ethanol and vaporized with an ultrasonic nebulizer into the vacuum chamber for trapping. The spheres were trapped at atmospheric pressure. Once a sphere was trapped, pressure in the chamber was reduced to the desired experimental level.

Particle size and displacement calibration. The particle size and displacement sensitivity of the apparatus can be calibrated with a measurement of the noise power spectral density with the particle at thermal equilibrium with the background gas and with zero feedback. The measured spectral density of the displacement noise for a single oscillatory mode is then given by the form

$$S(\Omega) = \frac{a\Gamma_0}{\left(\Omega_0^2 - \Omega^2\right)^2 + \Gamma_0^2\Omega^2} \tag{5}$$

where $\Gamma_0 = 2\gamma_g$ is the damping due to the background gas, $a = C^2 k_B T_0/\pi M$, k_B is Boltzmann's constant, T_0 is the temperature of the background gas, M is the mass of the particle and C is a constant with units V m^{-1}. Equation (5) takes a, Γ_0 and Ω_0 as free parameters. The constant C can then be determined with knowledge of the particle's mass. Measurements of the displacement noise power spectrum for calibration purposes were typically recorded at a chamber pressure of 10 mbar, such that $\Gamma_0 < \Omega_0$, which provides a well-resolved peak.

The size of the particle can be inferred directly from the measured damping rate, Γ_0. The damping rate for a particle with a radius comparable to or smaller than the mean free path of the gas, l, is given by[39]

$$\Gamma_0 = \frac{6\pi\mu r}{\rho_m (4\pi r^3/3)} \frac{0.619}{0.619 + \mathrm{Kn}} \left(1 + \frac{0.31}{0.785 + 1.152\ \mathrm{Kn} + \mathrm{Kn}^2}\right) \tag{6}$$

where μ is the dynamic viscosity of air, r is the particle's radius, ρ_m is the particle's material density, and $\mathrm{Kn} \equiv l/r$ is the Knudsen number. Solving equation (6) for r then provides a means to determine both the particle's radius as well as it's mass, $M = \rho_m(4\pi r^3/3)$. Values determined in this way can be compared with values provided by the manufacturer, which give the nominal particle radius to be 73.5 ± 2 nm. In this study, the particle was calibrated to have a radius of 68.3 ± 7 nm.

To ensure that only a single sphere was trapped, measurements of the natural damping rate were carried out for each centre-of-mass degree of freedom. A single spherical particle will experience equal damping along all three centre-of-mass degrees of freedom. However, multiple particles in the trap or non-spherical particle morphology can lead to unequal damping rates along the different axes, as well as additional degrees of freedom such as torsion and rotation.

Reporting Summary. Further information on research design is available in the Nature Research Reporting Summary linked to this article.

Data availability

The data that support the plots within this paper and other findings of this study are available from the corresponding authors upon reasonable request.

References

39. Beresnev, S. A., Chernyak, V. G. & Fomyagin, G. A. Motion of a spherical particle in a rarefied gas. Part 2. Drag and thermal polarization. *J. Fluid Mech.* **219**, 405–421 (1990).

nature research

Corresponding author(s): A. Nick Vamivakas

Lasing Reporting Summary

Nature Research wishes to improve the reproducibility of the work that we publish. This form is intended for publication with all accepted papers reporting claims of lasing and provides structure for consistency and transparency in reporting. Some list items might not apply to an individual manuscript, but all fields must be completed for clarity.

For further information on Nature Research policies, including our data availability policy, see Authors & Referees.

Experimental design

Please check: are the following details reported in the manuscript?

1. Threshold

Plots of device output power versus pump power over a wide range of values indicating a clear threshold	☒ Yes ☐ No	First paragraph of p. 4 and Figure 2a

2. Linewidth narrowing

Plots of spectral power density for the emission at pump powers below, around, and above the lasing threshold, indicating a clear linewidth narrowing at threshold	☒ Yes ☐ No	Supplementary Information section 4 and Figure S3
Resolution of the spectrometer used to make spectral measurements	☐ Yes ☒ No	Linewidth narrowing is demonstrated by measuring single side band phase noise of the phonon laser for frequency offsets > 10 Hz from the central oscillation frequency. The resolution of the measurement is ultimately determined by the sampling rate, rather than the resolution of a spectrometer.

3. Coherent emission

Measurements of the coherence and/or polarization of the emission	☒ Yes ☐ No	Final paragraph of p. 4 and Figure 2c

4. Beam spatial profile

Image and/or measurement of the spatial shape and profile of the emission, showing a well-defined beam above threshold	☐ Yes ☒ No	The phonon laser does not have a direct analogy to beam spatial profile in the sense that an optical laser does. However, we do measure the spatial position of the particle's centre-of-mass as it undergoes Brownian motion below threshold and coherent oscillation above threshold, shown in Figures 1b and 1c respectively. The measured profiles are consistent with each type of motion.

5. Operating conditions

Description of the laser and pumping conditions *Continuous-wave, pulsed, temperature of operation*	☒ Yes ☐ No	Beginning on p. 4 and in Figure 2 we discuss the continuous wave operation of the phonon laser, while on p. 6 and in Figure 3 we discuss the transient "turn-on" behavior of the phonon laser.
Threshold values provided as density values (e.g. W cm^{-2} or J cm^{-2}) taking into account the area of the device	☐ Yes ☒ No	Threshold values are reported in terms of the modulation depth on the trapping beam, which is directly accessible in the experiment. A full description of the experimental setup is provided in Supplementary Information section 1 and Figure S1.

6. Alternative explanations

Reasoning as to why alternative explanations have been ruled out as responsible for the emission characteristics *e.g. amplified spontaneous, directional scattering; modification of fluorescence spectrum by the cavity*	☐ Yes ☒ No	Fluorescence or directional scattering based explanations and do not apply to our phonon laser, nor is there a cavity. Amplified spontaneous emission is ruled out by the measurement of coherence (Figure 2c), as well as measurements of the phonon probability density (Figure 2d) and phase-space profile (Figure 2e), which are all consistent with laser operation.

7. Theoretical analysis

Theoretical analysis that ensures that the experimental values measured are realistic and reasonable *e.g. laser threshold, linewidth, cavity gain-loss, efficiency*	☒ Yes ☐ No	Discussion of the theoretical modeling of our phonon laser is found throughout the main text, particularly Equations 1-4. Further discussion of the modeling is found in Supplementary Information sections 2 and 3. We have found excellent agreement between experiment and theory.

8. Statistics

Number of devices fabricated and tested	☐ Yes ☒ No	Data from this paper has all been recorded on a single levitated silica nanosphere to ensure consistent calibration of the measurements . However, results have been reproduced consistently on well over 20 additional silica nanospheres. Additionally, we do provide data on two additional levitated silica nanophere phonon lasers of different mass to emphasize the generality of our setup. This can be found in Supplementary Information section 5.
Statistical analysis of the device performance and lifetime (time to failure)	☐ Yes ☒ No	In our experiments spheres can be held in the optical trap indefinitely, thus time to failure ,i.e. particle loss, is limited to human error.